

BIFURCATIONS OF LIOUVILLE TORI IN ELLIPTICAL BILLIARDS

VLADIMIR DRAGOVIĆ AND MILENA RADNOVIĆ

ABSTRACT. A detailed description of topology of integrable billiard systems is given. For elliptical billiards and geodesic billiards on ellipsoid, the corresponding Fomenko graphs are constructed.

CONTENTS

1. Introduction	1
2. Isoenergy Surfaces of Billiard Systems	2
3. Plane Elliptical Billiards	3
4. Billiards on Ellipsoids and Liouville surfaces	7
5. Billiards inside Ellipsoid in \mathbf{E}^3	10
Acknowledgements	13
Appendix: Fomenko graphs	13
References	17

1. INTRODUCTION

An important and geometrically significant class of dynamical systems consists of billiards with ellipsoidal boundary in \mathbf{E}^d . By Chasles theorem, any line in the d -dimensional space is tangent to exactly $d - 1$ quadrics from a given confocal family. These $d - 1$ caustics, confocal to the boundary of the billiard, are fixed for each segment of a given trajectory [2]. Existence of caustics is, in fact, a geometrical manifestation of integrals of motion. Due to them, we easily see that elliptical billiard is an completely integrable Hamiltonian system.

Famous classical example of integrable systems is geodesic flow on an ellipsoid \mathcal{E} in \mathbf{E}^d [19]. This system is closely related with billiards. In one way, the geodesic flow tends to the billiard flow inside an ellipsoid in \mathbf{E}^{d-1} when the smallest axis of \mathcal{E} tends to zero. On the other hand, the geodesic flow on \mathcal{E} is a limit of the billiard motion inside \mathcal{E} , when one of the caustics is a confocal ellipsoid tending to the boundary. Geodesic flow on ellipsoid also gives rise to another interesting class of billiard systems: billiards on the ellipsoid, where the boundary is determined by the intersection of the ellipsoid with a confocal quadric. Trajectories of such a billiard are composed of geodesic segments.

Billiard systems within and geodesic flows on ellipsoids have been extensively studied from XIXth century on: see classical works [10, 13, 19, 23, 26] and more recent ones [1, 3, 11, 12, 15, 16, 17, 18, 20, 24, 25, 27, 30] with the references therein.

From the non-vanishing interest, one may notice that this topic is far from being exhausted.

The object of this paper is to give topological description of such systems using Fomenko graphs. The detailed description of this kind of topological classification of integrable systems can be found in [7, 8, 9] and references therein, while a very concise summary for a reader not acquainted with it is given in the appendix of this paper. Although plane elliptical billiards are quite well known, we may see that such a description will give a new and exciting insight into its properties – note, for example, appearance of a non-orientable periodic trajectory along one of the axes of the billiard boundary in Proposition 3, see Figure 4.

In the book [7], one may find a large list of Fomenko graphs for known integrable systems, such as integrable cases of rigid body motion and integrable geodesic flows on surfaces. This paper provides an additional set of such examples. Some other examples, connected with near-integrable dynamics can be found in [29] while bifurcations of Liouville foliations in a certain class of integrable systems with two degrees of freedom, were classified using Fomenko graphs in [28].

Let us note that topological properties of elliptical billiards, viewed as discrete dynamical systems, have been recently studied in [30]. However, in this paper, we consider billiards as continuous systems, which enables us to use tools developed by Fomenko and his school.

This article is organized as follows. In Section 2, we begin with introductory remarks on isoenergy surfaces of billiard systems. Section 3 contains topological description of several examples of plane billiards, with the boundary composed of confocal conics, together with their representation via Fomenko graphs. In Section 4, topological description of the billiard flow with the quadratic boundary on the ellipsoid in \mathbf{E}^3 is given. We conclude this section by demonstrating the Liouville equivalence of the billiard motion within an ellipsoid on any Liouville surface. In Section 5, the topological structure of the billiard inside ellipsoid in \mathbf{E}^3 is described. The Appendix contains a summary on Fomenko graphs.

2. ISOENERGY SURFACES OF BILLIARD SYSTEMS

Let \mathcal{M}^n be an n -dimensional Riemann manifold, and $\Omega \subset \mathcal{M}$ a domain with the boundary composed of several smooth hypersurfaces. The billiard [22] inside Ω is a dynamical system where a material point of the unit mass is freely moving inside the domain and obeying the reflection law at the boundary, i.e. having congruent impact and reflection angles with the space tangent to the boundary at any bouncing point. It is also assumed that the reflection is absolutely elastic, i.e. that the speed of the material point does not change before and after impacts.

It is important to remark that the change of the total energy of the system, only the intensity of the velocity vector of the point will be changed while the trajectories will be the same at each energy level. That is why, for the complete analysis of the billiard system, we may fix the speed and investigate only one energy level.

The isoenergy space for the billiard system inside Ω is:

$$\begin{aligned} \mathcal{B} &= \{ (x, v) \mid x \in \Omega, v \in T_x\mathcal{M}, |v| = 1 \} / \sim, \\ (x, u) \sim (x, v) &\Leftrightarrow x \in \partial\Omega \text{ and } u - v \perp T_x\partial\Omega. \end{aligned}$$

Although the smoothness of motion of the billiard particle is violated at the boundary, let us note that, unexpectedly, the isoenergy space will be smooth, assuming that the billiard boundary is smooth. Even more, this manifold is smooth also when boundary is only composed of a few smooth parts, if the billiard reflection can be continuously defined at the angle points. This will be always the case in our examples, when the boundary is placed on a few confocal conics, since they are orthogonal to each other. Thus, the reflection at the intersection points is defined as follows: the velocity vector v after the reflection at the non-smooth point of the boundary, changes to $-v$.

3. PLANE ELLIPTICAL BILLIARDS

An important example of integrable billiard system is the billiard within an ellipse in \mathbf{E}^2 . The integrability of such a billiard motion is due to the nice and elementary fact: each segment of a trajectory is tangent to the same conic confocal with the boundary [2, 4]. Moreover, the boundary of any integrable billiard in a plane domain is composed of segments of several confocal conics [5].

In this section, we will describe the topology of the plane billiards with the elliptic boundary. We will use the Fomenko graphs [8] to represent the isoenergy surfaces.

Suppose that the ellipse in the plane is given by:

$$\mathcal{E} : \frac{x^2}{a} + \frac{y^2}{b} = 1, \quad a > b > 0.$$

The family of conics confocal with \mathcal{E} is:

$$\mathcal{C}_\mu : \frac{x^2}{a - \mu} + \frac{y^2}{b - \mu} = 1, \quad \mu \in \mathbf{R}.$$

We are going to consider billiard systems inside a bounded domain Ω in \mathbf{E}^2 , whose boundary is a union of arcs of several confocal conics. As in Introduction, we denote its isoenergy manifold by \mathcal{B} .

Proposition 1. *The isoenergy manifold corresponding to the billiard system within an ellipse in \mathbf{E}^2 is represented by the Fomenko graph on Figure 1.*

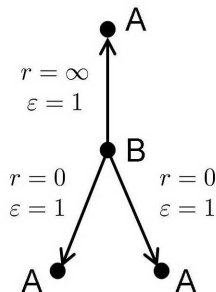


FIGURE 1. Fomenko graph corresponding to the billiard within an ellipse

The rotation functions corresponding to the edges of the graph are monotonous, and the limits of these functions on the lower edges are equal to ∞ approaching to

A-atom and 2 approaching to **B**-atom; on the upper edge the limit is ∞ approaching to **A**-atom and 1 approaching to **B**-atom.

Proof. The isoenergy manifold \mathcal{B} is the solid torus with the identification on \sim on the boundary. This identification glues pairs of points, while points contained on two curves – representing flows in positive and negative directions along the boundary of the billiard table, are not glued with any other. The torus with the two curves on the boundary is shown on Figure 2. These two curves correspond

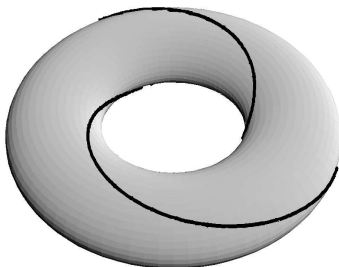


FIGURE 2. The isoenergy manifold for the billiard system within an ellipse

to the limit flow with the caustic $\mathcal{C}_0 = \mathcal{E}$, and they are represented with the lower **A**-atoms on the graph. For the parameter $0 < \mu < b$, i.e. when the caustic is an ellipse, we have two Liouville tori over each value of μ – one for each direction of rotation.

Let us describe the level set $\mu = b$. This level set contains exactly those billiard trajectories that pass through foci of the ellipse. Among them, there is one periodic trajectory – the motion along x -axis, while others have the well-known property that their segments alternately pass through left and right focus of the ellipse. These trajectories can be naturally divided into 2 classes – one is composed of the trajectories where the particle is moving upward through the left focus and downward through the right one, and the second contains the trajectories with the reverse property. Note these two classes by \mathcal{S}_1 and \mathcal{S}_2 respectively. All their trajectories are homoclinically tending to the x -axis, thus \mathcal{S}_1 and \mathcal{S}_2 are separatrices. Note that the periodic trajectory is orientable, so this level set corresponds to the **B**-atom.

Note that \mathcal{S}_1 (resp. \mathcal{S}_2) is the limit set of the family of Liouville tori corresponding to the flow with elliptic caustic in the clockwise (resp. counterclockwise) direction.

When $b < \mu < a$, i.e. when the caustic is a hyperbola, there is only one torus for each value. Finally, to the $\mu = a$, the periodic motion along y -axis takes place, and it is represented by the upper **A**-atom. \square

In the similar way, we can obtain the following:

Proposition 2. *The isoenergy manifold corresponding to the billiard system in the domain limited with two confocal ellipses in \mathbf{E}^2 is represented by the Fomenko graph on Figure 3.*

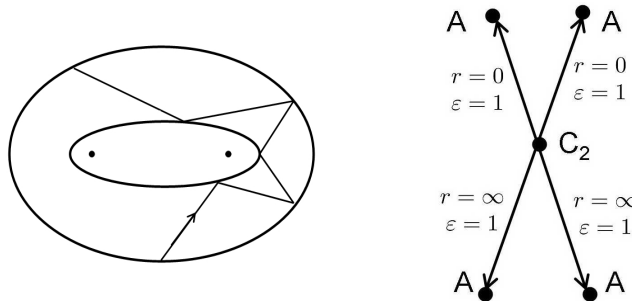


FIGURE 3. Billiard between two confocal ellipses and its Fomenko graph

Proof. As in Proposition 1, the lower A -atoms correspond to the limit flows on the boundary of the outer ellipse.

The level set for the caustic $\mu = b$ contains two periodic trajectories placed on the x -axis and all trajectories such that the continuations of their segments contain the foci. Let us note that such a trajectory is heteroclinic and placed only in one of the half-planes with the x -axis as the edge. Thus, this level set has four separatrices: two in the upper half-plane, two in the lower one. In each half-plane, one separatrix contains trajectories tending to the left periodic trajectory on the x -axis when time tends to ∞ and to the right one in $-\infty$, and opposite for orbits on the other separatrix. Liouville tori corresponding to elliptic caustics tend when μ tends to b , to two separatrices with the same movement direction – clockwise or counterclockwise.

For hyperbolic caustics, the billiard table become split into two domains, symmetric with respect to the x -axis. Each family of Liouville tori tend to the two separatrices from the level $\mu = b$ that are contained in the same half-plane.

This analysis shows that the atom that describes level set $\mu = b$ is C_2 .

The upper A -atoms correspond to the periodic orbits along y -axis. □

Now we will consider the domain is determined by an ellipse and a confocal hyperbola. Let us note that the phase space in the cases, where the boundary is not smooth at every point, must be considered with a special attention. Since confocal conics are always orthogonal in the intersection points, the periodic flows along smooth arcs may appear as limits of the billiard motion, when the caustic tend to the conic containing the arc. Thus, although the tangent space to the boundary in the intersection points is not defined, we will take that the “allowed” velocity vectors in such points are those tangent to the curves containing these points, with the opposite vectors identified with each other.

Proposition 3. *Consider the billiard domain with the border composed of an ellipse and a confocal hyperbola. Then:*

- 1 *If the domain is outside hyperbola, then the isoenergy manifold is represented by the graph on Figure 4.*
- 2 *If the domain is inside hyperbola, then the isoenergy manifold is represented by the graph on Figure 5.*

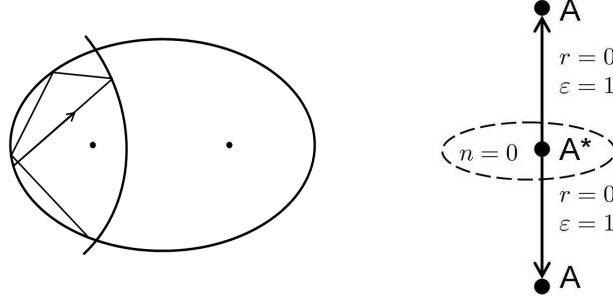


FIGURE 4. Billiard between ellipse and one branch of hyperbola and its Fomenko graph

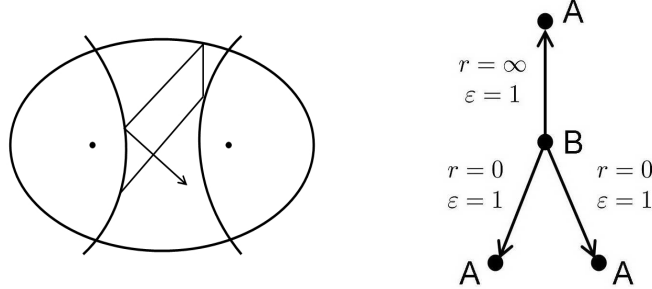


FIGURE 5. Billiard inside ellipse and hyperbola and its Fomenko graph

Proof. In the first case, each of the **A**-atoms corresponds to the limit periodic orbit along one of the smooth arcs constituting the boundary of the billiard domain. The **A***-atom represents the periodic orbit along x -axis and its homoclinic trajectories.

In the second case, the lower **A**-atoms correspond to the limit motion on two arcs of the ellipse, the **B**-atom to the periodic orbit on x -axis and its homoclinic orbits, and the upper **A** atom to periodic orbit along y -axis. It is interesting to note that this system is Liouville equivalent to the billiard within the ellipse (compare Figures 1 and 5). \square

We conclude this section by analyzing an example when the border of the billiard table is continuously changed, to see how the bifurcations in the isoenergy manifolds appear.

Proposition 4. *Consider a billiard domain limited by two confocal ellipses and two arcs contained in different branches of a confocal hyperbola.*

- 1 If the domain is inside the hyperbola, then the isoenergy manifold is represented by the graph on Figure 6.
- 2 If the x -axis is a part of the boundary, then the isoenergy manifold is represented by the graph on Figure 7. Note that **V** corresponds to a degenerated singular leaf containing two orientable periodic orbits and two heteroclinic separatrices.
- 3 If the domain is as shown on the left side of Figure 8, then the isoenergy manifold is represented by the graph on the right side of Figure 8.

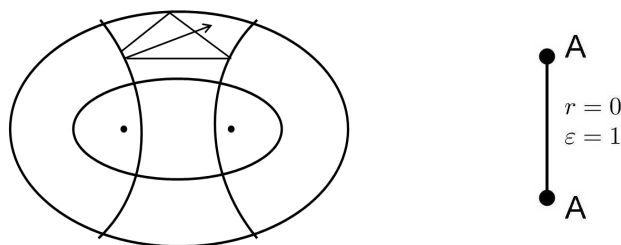


FIGURE 6. Billiard motion between two ellipses and hyperbola and the corresponding Fomenko graph

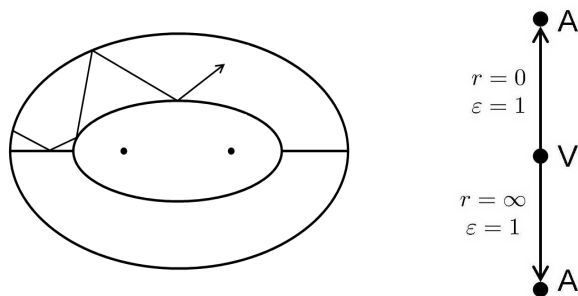


FIGURE 7. Billiard motion between two ellipses and a degenerate hyperbola with the Fomenko graph

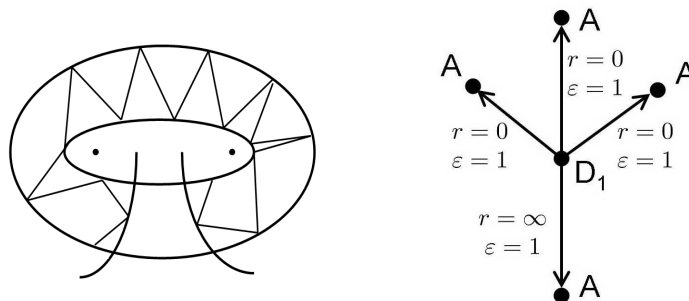


FIGURE 8. Billiard motion between two ellipses and hyperbola and the corresponding Fomenko graph

4. BILLIARDS ON ELLIPSOIDS AND LIOUVILLE SURFACES

In this section, we are going to analyze the topology of the billiard motion on the ellipsoid in \mathbf{E}^3 , with the boundary cut by a confocal quadric surface. Next, we will consider the billiards within generalized ellipses on Liouville surfaces. Obtained results are going to be compared with those from the previous section.

4.1. Topology of Geodesic Motion on Ellipsoid in \mathbf{E}^3 . Since the segments of billiard trajectories on the ellipsoid are placed on geodesic lines, it is essential to

consider topology of the isoenergy surfaces for the geodesic motion on the ellipsoid. This topology is completely described in [6].

We suppose that the ellipsoid in \mathbf{E}^3 is given by the equation:

$$(1) \quad \mathcal{E} : \frac{x^2}{a} + \frac{y^2}{b} + \frac{z^2}{c} = 1, \quad 0 < c < b < a.$$

Theorem 1. [[6, 7]] *The Fomenko graph for the Jacobi problem of geodesic lines on an ellipsoid is presented in Figure 9. The rotation function that correspond to*

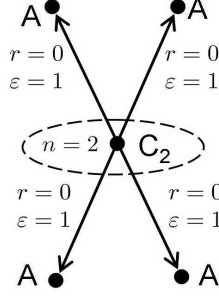


FIGURE 9. Fomenko graph for the Jacobi problem

the lower and upper edges of the graph are:

$$\rho_{\text{lower}}(\alpha) = \frac{\int_c^\alpha \Phi(\lambda, \alpha) d\lambda}{\int_b^a \Phi(\lambda, \alpha) d\lambda} \quad (\alpha \in (c, b)), \quad \rho_{\text{upper}}(\alpha) = \frac{\int_c^b \Phi(\lambda, \alpha) d\lambda}{\int_\alpha^a \Phi(\lambda, \alpha) d\lambda} \quad (\alpha \in (b, a)),$$

where

$$\Phi(\lambda, \alpha) = \frac{\lambda}{\sqrt{-\lambda(a-\lambda)(b-\lambda)(c-\lambda)(\alpha-\lambda)}}.$$

It is interesting to remark that this theorem is used to prove that the Jacobi problem of geodesic lines on an ellipsoid and the Euler case of the rigid body motion are orbitally equivalent (see [6, 7]).

4.2. Billiards on Ellipsoid in \mathbf{E}^3 . A generalized ellipse on the surface of the ellipsoid (1) is the intersection of this ellipsoid with a confocal hyperboloid. Let us note that such an intersection consists of two disjoint closed curves, which are curvature lines on the ellipsoid. This intersection divides the surface of the ellipsoid into three domains: two of them are simply connected and congruent to each other, while the third one, placed between them is 1-connected.

More precisely, any surface confocal with the ellipsoid (1) is given by the equation of the form (see Figure 10):

$$(2) \quad \mathcal{Q}_\lambda : Q_\lambda = \frac{x^2}{a-\lambda} + \frac{y^2}{b-\lambda} + \frac{z^2}{c-\lambda} = 1.$$

Let the Jacobi coordinates $(\lambda_1, \lambda_2, \lambda_3)$ related to this system of confocal quadric surfaces be ordered by the condition $\lambda_1 > \lambda_2 > \lambda_3$.

Then the one-sheeted hyperboloid \mathcal{Q}_β , ($c < \beta < b$), cuts out the following three domains on the surface of \mathcal{E} : $\Omega_1^\beta = \{\lambda_2 > \beta, z > 0\}$, $\Omega_2^\beta = \{\lambda_2 > \beta, z < 0\}$ and

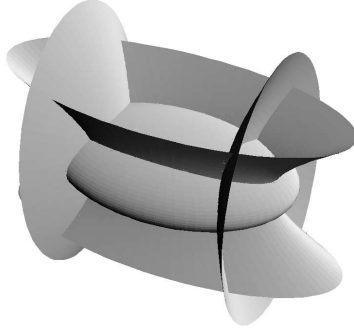


FIGURE 10. Confocal quadrics

$\Omega_3^\beta = \{\lambda_2 < \beta\}$. The first two domains are symmetric with respect to the xy -plane, and the third one is the ring placed between them on \mathcal{E} , as shown on Figure 11.

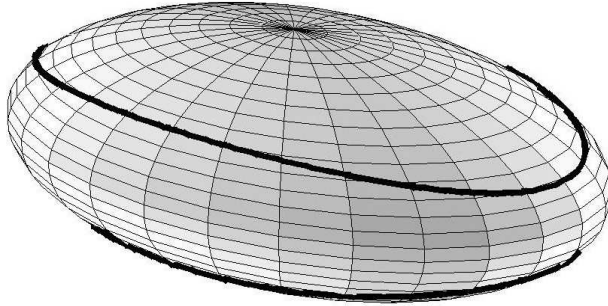


FIGURE 11. Intersection of ellipsoid with one-sheeted hyperboloid

Similarly, the two-sheeted hyperboloid \mathcal{Q}_γ , ($b < \gamma < a$), determines the domains $\Omega_1^\gamma = \{\lambda_1 < \gamma, x > 0\}$, $\Omega_2^\gamma = \{\lambda_1 < \gamma, x < 0\}$ and $\Omega_3^\gamma = \{\lambda_1 > \gamma\}$, see Figure 12.

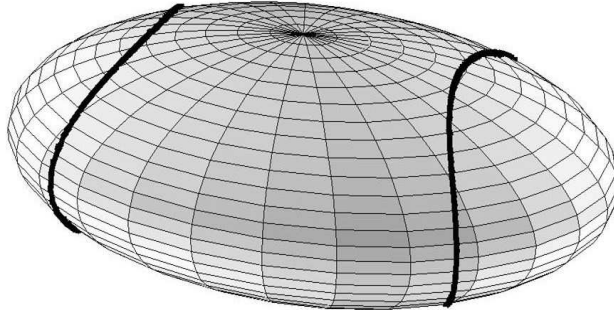


FIGURE 12. Intersection of ellipsoid with two-sheeted hyperboloid

Proposition 5. *The isoenergy manifolds corresponding to the billiard systems within the domains Ω_1^β and Ω_1^γ on \mathcal{E} is represented by the Fomenko graph on Figure 1.*

The rotation functions for the billiard within Ω_1^β , for the lower and upper edges of the Fomenko graph respectively, are:

$$\rho_{\text{lower}}^\beta(\alpha) = \frac{\int_\beta^\alpha \Phi(\lambda, \alpha)}{\int_b^a \Phi(\lambda, \alpha)} \quad (\alpha \in (\beta, b)), \quad \rho_{\text{upper}}^\beta(\alpha) = \frac{\int_\beta^b \Phi(\lambda, \alpha)}{\int_\alpha^a \Phi(\lambda, \alpha)} \quad (\alpha \in (b, a)).$$

The rotation functions for the billiard within Ω_1^γ , for the lower and upper edges of the Fomenko graph respectively, are:

$$\rho_{\text{lower}}^\gamma(\alpha) = \frac{\int_\alpha^\gamma \Phi(\lambda, \alpha)}{\int_c^b \Phi(\lambda, \alpha)} \quad (\alpha \in (b, \gamma)), \quad \rho_{\text{upper}}^\gamma(\alpha) = \frac{\int_b^\gamma \Phi(\lambda, \alpha)}{\int_c^\alpha \Phi(\lambda, \alpha)} \quad (\alpha \in (c, b)).$$

Φ is defined as in Theorem 1.

4.3. Billiard within an Ellipse on a Liouville surface. Now, let us state the main result of this section.

Theorem 2. *All billiard systems within ellipse on an arbitrary Liouville surface are Liouville equivalent. The Fomenko graph corresponding to an isoenergy manifold of such a system is represented on Figure 1.*

Proof. Families of confocal ellipses and hyperbolas, together with corresponding billiard systems, were defined and described by Darboux [13] (for a recent account on this topic, see [15, 16]). Since such billiard have all topological properties analogous to billiards within an ellipse in the Euclidean plane, the theorem is proved. \square

5. BILLIARDS INSIDE ELLIPSOID IN \mathbf{E}^3

Here, we are going to analyze the topology of the billiard motion within an ellipsoid in \mathbf{E}^3 . We suppose that the equation of the ellipsoid is (1).

Each trajectory of the billiard motion within \mathcal{E} has exactly two caustics from the confocal family \mathcal{Q}_λ . Suppose these two surfaces are \mathcal{Q}_{λ_1} and \mathcal{Q}_{λ_2} , $\lambda_2 \leq \lambda_1$. Then the bifurcation set of an isoenergy surface of the system is given on Figure 13.

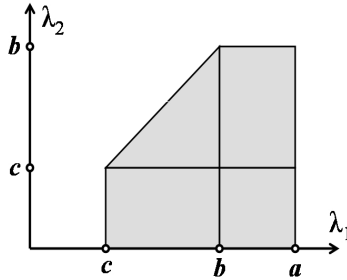


FIGURE 13. The bifurcation set for the billiard within an ellipsoid in \mathbf{E}^3

The bifurcations of the Liouville tori for this system were investigated in [21, 3, 14].

Now, let us explain in detail how the behaviour of the billiard motion is connected to the diagram on Figure 13.

Over each point in the gray area on the diagram, there is one or two 3-dimensional Liouville tori. The marked edges will correspond to the degenerated level sets.

Now, let us describe in detail the level sets lying over different points in the bifurcation set on the Figure 13.

5.1. Regular Leaves. Over each point inside rectangles $[c, b] \times [0, c]$, $[b, a] \times [0, c]$ and the triangle with vertices (c, c) , (b, c) , (b, b) , there are two Liouville tori \mathbf{T}^3 . Over each point inside rectangle $[b, a] \times [c, b]$, there is only one \mathbf{T}^3 .

- Points inside $[c, b] \times [0, c]$ correspond to the motion with an ellipsoid and a one-sheeted hyperboloid as caustics. One Liouville torus is formed by the trajectories winding in the positive direction around the z -axis, and the other one by those winding in the negative direction.
- Points inside $[b, a] \times [0, c]$ correspond to the case when one caustic is ellipsoid and the other a two-sheeted hyperboloid. Each Liouville torus is formed by the trajectories winding in one direction around the x -axis.
- Points inside triangle $(c, c) - (b, c) - (b, b)$ correspond to the motion with both caustics being different one-sheeted hyperboloids. Each of the Liouville tori is formed by the trajectories winding in one direction around the x -axis.
- Points inside rectangle $[b, a] \times [c, b]$ correspond to the case when both caustics are hyperboloids, but of different type. Then, all corresponding billiard trajectories form one Liouville torus.

5.2. Singular Leaves. Singular leaves are lying over edges of the diagram represented on Figure 13. They appear when one or both caustics are degenerated.

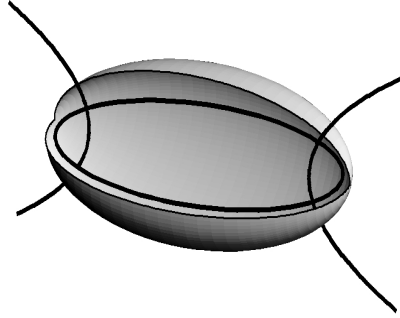
First, let us clarify the notion of a degenerated quadric from confocal family (2), as well as the geometrical meaning of the billiard motion with such a caustic.

The degenerated quadrics \mathcal{Q}_λ , $\lambda \in \{a, b, c\}$ are the following curve lying in the coordinate planes:

$$\begin{aligned} \mathcal{Q}_a &: -\frac{y^2}{a-b} - \frac{z^2}{a-c} = 1, \quad x = 0, \\ \mathcal{Q}_b &: \frac{x^2}{a-b} - \frac{z^2}{b-c} = 1, \quad y = 0, \\ \mathcal{Q}_c &: \frac{x^2}{a-c} + \frac{y^2}{b-c} = 1, \quad z = 0. \end{aligned}$$

Notice that \mathcal{Q}_c is an ellipse in the xy -plane, \mathcal{Q}_b is a hyperbola in the xz -plane, while \mathcal{Q}_a is, in the real case, the empty set. Nevertheless, we will consider \mathcal{Q}_a as an abstract curve in the yz -plane. The degenerated quadrics are depicted on Figure 14.

The billiard motion with some of these three degenerated caustics \mathcal{Q}_λ is either such that each segment of the trajectory intersects the curve \mathcal{Q}_λ or the whole trajectory is lying in the coordinate plane containing this curve. In the latter case,

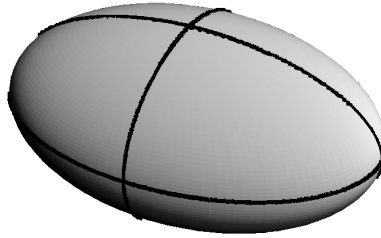
FIGURE 14. Ellipsoid \mathcal{E} and degenerated quadrics $\mathcal{Q}_b, \mathcal{Q}_c$

the motion reduces to the plane billiard one of the ellipses:

$$\begin{aligned}\mathcal{E}_a &: \frac{y^2}{b} + \frac{z^2}{c} = 1, \quad x = 0, \\ \mathcal{E}_b &: \frac{x^2}{a} + \frac{z^2}{c} = 1, \quad y = 0, \\ \mathcal{E}_c &: \frac{x^2}{a} + \frac{y^2}{b} = 1, \quad z = 0.\end{aligned}$$

Notice that, in the case $\lambda = a$, only plane trajectories exist.

Each of these three ellipses is the intersection of \mathcal{E} with one of the coordinate hyper-planes (see Figure 15).

FIGURE 15. Ellipsoid \mathcal{E} and ellipses $\mathcal{E}_a, \mathcal{E}_b, \mathcal{E}_c$

Besides these cases with a degenerated caustic, there one more special case – when one of the caustics is the boundary ellipsoid \mathcal{E} . This case can be considered as the limit case with the caustic \mathcal{Q}_λ , $\lambda \rightarrow 0_+$, and its trajectories are geodesic lines on \mathcal{E} .

Now, let us analyze the edges of the bifurcation diagram on Figure 13.

Edge $[c, a] \times \{0\}$. As already mentioned, the motion corresponding to this edge is the geodesic motion on \mathcal{E} . Thus, the topology of the corresponding subset in the isoenergy manifold is completely described by the Fomenko graph on Figure 9.

Let us summarize this case:

- Point $(c, 0)$ corresponds to the motion along the curve \mathcal{E}_c . There are two 1-dimensional tori \mathbf{T}^1 lying over the point $(c, 0)$ of the bifurcation diagram – each one corresponding to the flow in one direction.
- Inner points of the segment $[c, b]$ on λ_1 -axis correspond to the geodesic motion on \mathcal{E} with a one-sheeted hyperboloid as caustic. Such geodesic lines fill the ring between two intersection curves of \mathcal{E} and the hyperboloid. Over each point inside the segment, there are two tori \mathbf{T}^2 – each one corresponding to winding in one direction around the z -axis.
- The level set corresponding to $(b, 0)$ contains two periodic trajectories and four two-dimensional separatrices. The periodic trajectories are placed along the curve \mathcal{E}_b . Trajectories on the separatrices are passing through the umbilical points of the ellipsoid.
- Inner points of the segment $[b, a]$ on λ_1 -axis correspond to the geodesic motion on \mathcal{E} with a two-sheeted hyperboloid as caustic. Such geodesic lines fill the ring between two intersection curves of \mathcal{E} and the hyperboloid. Over each point inside the segment, there are two tori \mathbf{T}^2 – each one corresponding to winding in one direction around the x -axis.
- Point $(a, 0)$ corresponds to the motion along \mathcal{E}_a . There are two 1-dimensional tori \mathbf{T}^1 lying over this point – each one corresponding to the motion in one direction.

Edge $\{a\} \times [0, b]$. This edge corresponds to the billiard motion with the degenerated caustic \mathcal{Q}_a . All trajectories of such a motion are placed in the yz -plane, thus this edge in fact corresponds to the billiard within an ellipse. The topology of the set lying over this edge is completely described by the Fomenko atom on Figure 1.

Edge $[b, a] \times \{b\}$. This edge corresponds to the billiard motion with one degenerate caustic \mathcal{Q}_b , and the other caustic being a two-sheeted hyperboloid.

Acknowledgements. We thank A. V. Bolsinov for interesting discussions. This work is partially supported by the Serbian Ministry of Science and Technology, Project no. 144014: *Geometry and Topology of Manifolds and Integrable Dynamical Systems*.

APPENDIX: FOMENKO GRAPHS

In the appendix, we are going to give a concise description of the representation of isoenergy surfaces and some of their topological invariants by Fomenko graphs. For all details, see [6, 9] and references therein.

Let $(\mathcal{M}, \omega, H, K)$ be an integrable system given on a four-dimensional manifold with a symplectic form ω . Here H, K denote independent functions on \mathcal{M} , commuting with respect to the symplectic structure on \mathcal{M} .

Level sets are subsets of \mathcal{M} given by equations $H = \text{const}, K = \text{const}$. The *Liouville foliation* of \mathcal{M} is its decomposition into connected components of the level sets. A leave of the foliations is *regular* if dH, dK are independent at each its point, otherwise it is called *singular*. Singular leaves satisfying some additional conditions will be called *non-degenerate*. For these non-degeneracy conditions, see [6].

We suppose that *isoenergy surface* $H = \text{const}$ are compact, thus each foliation leaf will also be compact. Thus, by the Arnol'd-Liouville theorem [2], each regular leaf is diffeomorphic to the 2-dimensional torus \mathbf{T}^2 and the motion in its neighborhood is completely described by, for example, the action-angle coordinates. We say that isoenergy surfaces are *Liouville equivalent* if they are topologically conjugate and the homeomorphism preserves their Liouville foliations

The set of topological invariants that describe completely isoenergy manifolds containing regular and non-degenerate leaves not containing fixed points of , up to their Liouville equivalence, consists of:

- *The oriented graph* G , whose vertices correspond to the singular connected components of the level sets of K , and edges to one-parameter families of Liouville tori;
- *The collection of Fomenko atoms*, such that each atom marks exactly one vertex of the graph G ;
- *The collection of pairs of numbers* (r_i, ε_i) , with $r_i \in ([0, 1) \cap \mathbf{Q}) \cup \{\infty\}$, $\varepsilon_i \in \{-1, 1\}$, $1 \leq i \leq n$. Here, n is the number of edges of the graph G and each pair (r_i, ε_i) marks an edge of the graph;
- *The collection of integers* n_1, n_2, \dots, n_s . The numbers n_k correspond to certain connected components of the subgraph G^0 of G . G^0 consists of all vertices of G and the edges marked with $r_i = \infty$. The connected components marked with integers n_k are those that do not contain a vertex corresponding to an isolated critical circle (an **A** atom) on the manifold \mathcal{Q} .

Let us clarify the meaning of these invariants.

First, we are going to describe the construction of the graph G from the manifold \mathcal{Q} . Each singular leaf of the Liouville foliation corresponds to exactly one vertex of the graph. If we cut \mathcal{Q} along such leaves, the manifold will fall apart into connected sets, each one consisting of one-parameter family of Liouville tori. Each of these families is represented by an edge of the graph G . The vertex of G which corresponds to a singular leaf \mathcal{L} is incident to the edge corresponding to the family \mathcal{T} of tori if and only if $\partial\mathcal{T} \cap \mathcal{L}$ is non empty.

Note that $\partial\mathcal{T}$ has two connected components, each corresponding to a singular leaf. If the two singular leaves coincide, then the edge creates a loop connecting one vertex to itself.

Now, when the graph is constructed, one need to add the orientation to each edge. This may be done arbitrarily, but, once determined, the orientation must stay fixed because the values of numerical Fomenko invariants depend on it.

The Fomenko atom which corresponds to a singular leaf \mathcal{L} of a singular level set is determined by the topological type of the set \mathcal{L}_ε . The set $\mathcal{L}_\varepsilon \supset \mathcal{L}$ is the connected component of $\{ p \in \mathcal{Q} \mid c - \varepsilon < K(p) < c + \varepsilon \}$, where $c = K(\mathcal{L})$, and $\varepsilon > 0$ is such that c is the only critical value of the function K on \mathcal{Q} in interval $(c - \varepsilon, c + \varepsilon)$.

Let $\mathcal{L}_\varepsilon^+ = \{ p \in \mathcal{L}_\varepsilon \mid K(p) > c \}$, $\mathcal{L}_\varepsilon^- = \{ p \in \mathcal{L}_\varepsilon \mid K(p) < c \}$. Each of the sets $\mathcal{L}_\varepsilon^+$, $\mathcal{L}_\varepsilon^-$ is a union of several connected components, each component being a one-parameter family of Liouville tori. Each of these families corresponds to the beginning of an edge of the graph G incident to the vertex corresponding to \mathcal{L} .

Let us say a few words on the topological structure of the set \mathcal{L} . This set consists of at least one fixed point or closed one-dimensional orbit of the Poisson action Φ

on \mathcal{M} and several (possibly none) two-dimensional orbits of the action, which are called *separatrices*.

The trajectories on each of these two-dimensional separatrices is homoclinically or heteroclinically tending to the lower-dimensional orbits. The Liouville tori of each of the families in $\mathcal{L}_\varepsilon \setminus \mathcal{L} = \mathcal{L}_\varepsilon^+ \cup \mathcal{L}_\varepsilon^-$ tend, as the integral K approaches c , to a closure of a subset of the separatrix set.

Fomenko Atoms. Fomenko and his school completely described and classified non-degenerate leaves that do not contain fixed points of the Hamiltonian H .

If \mathcal{L} is not an isolated critical circle, then a sufficiently small neighborhood of each 1-dimensional orbit in \mathcal{L} is isomorphic to either two cylinders intersecting along the base circle, and then the orbit is *orientable*, or to two Moebius bands intersecting each other along the joint base circle, then the 1-dimensional orbit is *non-orientable*.

The number of closed one-dimensional orbits in \mathcal{L} is called *the complexity* of the corresponding atom.

Fomenko atoms of complexity 1. There are exactly three such atoms.

The atom A. This atom corresponds to a normally elliptic singular circle, which is isolated on the isoenergy surface \mathcal{Q} . A small neighborhood of such a circle in \mathcal{Q} is diffeomorphic to a solid torus. One of the sets $\mathcal{L}_\varepsilon^+$, $\mathcal{L}_\varepsilon^-$ is empty, the other one is connected. Thus only one edge of the graph G is incident with the vertex marked with the letter atom **A**.

The atom B. In this case, \mathcal{L} consists of one orientable normally hyperbolic circle and two 2-dimensional separatrices – it is diffeomorphic to a direct product of the circle \mathbf{S}^1 and the plane curve given by the equation $y^2 = x^2 - x^4$. Because of its shape, we will refer to this curve as the ‘*figure eight*’. The set $\mathcal{L}_\varepsilon \setminus \mathcal{L}$ has 3 connected components, two of them being placed in $\mathcal{L}_\varepsilon^+$ and one in $\mathcal{L}_\varepsilon^-$, or vice versa. Let us fix that two of them are in $\mathcal{L}_\varepsilon^+$. Each of these two families of Liouville tori limits as K approaches c to only one of the separatrices. The tori in $\mathcal{L}_\varepsilon^-$ tend to the union of the separatrices.

The atom A.* \mathcal{L} consists of one non-orientable hyperbolic circle and one 2-dimensional separatrix. It is homeomorphic to the smooth bundle over \mathbf{S}^1 with the ‘figure eight’ as fiber and the structural group consisting of the identity mapping and the central symmetry of the ‘figure eight’. Both $\mathcal{L}_\varepsilon^+$ and $\mathcal{L}_\varepsilon^-$ are 1-parameter families of Liouville tori, one limiting to the separatrix from outside the ‘figure eight’ and the other from the interior part of the ‘figure eight’.

Fomenko atoms of complexity 2. There are six such atoms. However, we give here the description only of those appearing in the examples of this paper, see Figures 3, 8, 9.

The atom C₂. \mathcal{L} consists of two orientable circles γ_1 , γ_2 and four heteroclinic 2-dimensional separatrices \mathcal{S}_1 , \mathcal{S}_2 , \mathcal{S}_3 , \mathcal{S}_4 . Trajectories on \mathcal{S}_1 , \mathcal{S}_3 are approaching γ_1 as time tend to ∞ , and γ_2 as time tend to $-\infty$, while those placed on \mathcal{S}_2 , \mathcal{S}_4 approach γ_2 as time tend to ∞ , and γ_1 as time tend to $-\infty$. Each of the sets $\mathcal{L}_\varepsilon^+$, $\mathcal{L}_\varepsilon^-$ contains two families of Liouville tori. As K approaches to c , the tori from one

family in $\mathcal{L}_\varepsilon^-$ deform to $\mathcal{S}_1 \cup \mathcal{S}_2$, and from the other one to $\mathcal{S}_3 \cup \mathcal{S}_4$. The tori from one family in $\mathcal{L}_\varepsilon^+$ is deformed to $\mathcal{S}_1 \cup \mathcal{S}_4$, and from the other to $\mathcal{S}_2 \cup \mathcal{S}_3$.

The atom \mathbf{D}_1 . \mathcal{L} consists of two orientable circles γ_1, γ_2 and four 2-dimensional separatrices $\mathcal{S}_1, \mathcal{S}_2, \mathcal{S}_3, \mathcal{S}_4$. Trajectories of $\mathcal{S}_1, \mathcal{S}_2$ homoclinically tend to γ_1, γ_2 respectively. Trajectories on \mathcal{S}_3 are approaching γ_1 as time tend to ∞ , and γ_2 as time tend to $-\infty$, while those placed on \mathcal{S}_4 , approach γ_2 as time tend to ∞ , and γ_1 as time tend to $-\infty$. One of the sets $\mathcal{L}_\varepsilon^+, \mathcal{L}_\varepsilon^-$ contains three, and the other one family of Liouville tori. Lets say that $\mathcal{L}_\varepsilon^+$ contains three families. As K approaches to c , these families deform to $\mathcal{S}_1, \mathcal{S}_2$ and $\mathcal{S}_3 \cap \mathcal{S}_4$ respectively, while the family contained in $\mathcal{L}_\varepsilon^-$ deform to the whole separatrix set.

This concludes the complete list of all atoms appearing in this paper.

Numerical Fomenko Invariants. Each edge of the Fomenko graph corresponds to a one-parameter family of Liouville tori. Let us cut each of these families along one Liouville torus. The manifold \mathcal{Q} will disintegrate into pieces, each corresponding to the singular level set, i.e. to a part of the Fomenko graph containing only one vertex and the initial segments of the edges incident to this vertex. To reconstruct \mathcal{Q} from these pieces, we need to identify the corresponding boundary tori. This can be done in different ways. Thus, the basis of cycles is fixed in a certain canonical way on each boundary torus. Denote by b_i^-, b_i^+ the bases corresponding to the beginning and the end of an edge respectively. Denote by:

$$\begin{pmatrix} \alpha_i & \beta_i \\ \gamma_i & \delta_i \end{pmatrix}$$

the transformation matrix from b_i^- to b_i^+ .

Marks r_i . They are defined as:

$$r_i = \begin{cases} \left\{ \begin{matrix} \alpha_i \\ \beta_i \end{matrix} \right\}, & \text{if } \beta_i \neq 0, \\ \infty, & \text{if } \beta_i = 0. \end{cases}$$

Marks ε_i . They are:

$$\varepsilon_i = \begin{cases} \text{sign } \beta_i, & \text{if } \beta_i \neq 0, \\ \text{sign } \alpha_i, & \text{if } \beta_i = 0. \end{cases}$$

Marks n_k . To determine marks n_k , we cut all the edges of the graphs having finite marks r_i . In this way the graph will fall apart into a few connected parts. Consider only parts not containing \mathbf{A} -atoms. To each edge of the graph having a vertex in a given connected part, we join the following integer:

$$\Theta_i = \begin{cases} \begin{bmatrix} \alpha_i \\ \beta_i \end{bmatrix}, & \text{if } e_i \text{ is has the initial vertex in the connected part} \\ \begin{bmatrix} -\delta_i \\ \beta_i \end{bmatrix}, & \text{if } e_i \text{ is has the ending vertex in the connected part} \\ \begin{bmatrix} -\gamma_i \\ \alpha_i \end{bmatrix}, & \text{if both vertexes of } e_i \text{ are in the connected part.} \end{cases}$$

Then to the connected part of the graph, we join the mark:

$$n_k = \sum \Theta_i.$$

Rotation Functions. Consider an arbitrary edge of a given Fomenko graph and recall that it represents a one-parameter family of Liouville tori. Let us choose one such a torus and fix on it a basis (λ, μ) of cycles. By Arnol'd-Liouville theorem, the motion on the torus is linear, thus there are coordinates $(\varphi_1, \varphi_2) \in \mathbf{S}^1 \times \mathbf{S}^1$ such that the Hamiltonian vector field can be written in the form:

$$a \frac{\partial}{\partial \varphi_1} + b \frac{\partial}{\partial \varphi_2},$$

while the coordinate lines $\varphi_2 = \text{const}$, $\varphi_1 = \text{const}$ are equivalent to basic cycles λ , μ . *Rotation number* on the torus is $\rho = \frac{a}{b}$. If we continuously extend the basis (λ, μ) to the other tori of the family, the collection of obtained rotation numbers will represent *rotation function*.

REFERENCES

- [1] S. Abenda, Yu. Fedorov, *Closed geodesics and billiards on quadrics related to elliptic KdV solutions*, Letters in Mathematical Physics **76** (2006), 111–134.
- [2] V. Arnol'd, *Mathematical Methods of Classical Mechanics*, Springer-Verlag, New York, 1978.
- [3] M. Audin, *Courbes algébriques et systèmes intégrables: géodésiques des quadriques*, Expo. Math. **12** (1994), 193–226.
- [4] M. Berger, *Geometry*, Springer-Verlag, Berlin, 1987.
- [5] S. V. Bolotin, *Integrable Birkhoff billiards*, Vestnik Moskov. Univ. Ser. I Mat. Mekh. (1990), no. 2, 33–36, 105.
- [6] A. V. Bolsinov, A. T. Fomenko, *The geodesic flow of an ellipsoid is orbitally equivalent to the Euler integrable case in the dynamics of a rigid body*, Dokl. Akad. Nauk SSSR **339** (1994), no. 3, 293–296.
- [7] A. V. Bolsinov, A. T. Fomenko, *Integrable Hamiltonian Systems: Geometry, Topology, Classification*, Chapman and Hall/CRC, Boca Raton, FL, 2004.
- [8] A. V. Bolsinov, S. V. Matveev, A. T. Fomenko, *Topological classification of integrable Hamiltonian systems with two degrees of freedom. List of systems with small complexity*, Russian Math. Surveys **45** (1990), vol. 2, 59–94.
- [9] A. V. Bolsinov, A. A. Oshemkov, *Singularities of integrable Hamiltonian systems*, In: Topological Methods in the Theory of Integrable Systems, Cambridge Scientific Publ., 2006, pp. 1–67.
- [10] A. Cayley, *Developments on the porism of the in-and-circumscribed polygon*, Philosophical magazine **7** (1854), 339–345.
- [11] S.-J. Chang, B. Crespi B, K.-J. Shi, *Elliptical billiard systems and the full Poncelet's theorem in n dimensions*, J. Math. Phys. **34** (1993), no. 6, 2242–2256.
- [12] S.-J. Chang, K. J. Shi, *Billiard systems on quadric surfaces and the Poncelet theorem*, J. Math. Phys. **30** (1989), no. 4, 798–804.
- [13] G. Darboux, *Leçons sur la théorie générale des surfaces et les applications géométriques du calcul infinitesimal*, volumes 2 and 3, Gauthier-Villars, Paris, 1887, 1889.
- [14] A. Delshams, Y. Fedorov, R. Ramírez-Ros, *Homoclinic billiard orbits inside symmetrically perturbed ellipsoids*, Nonlinearity **14** (2001), 1141–1195.
- [15] V. Dragović, M. Radnović, *Geometry of integrable billiards and pencils of quadrics*, Journal Math. Pures Appl. **85** (2006), 758–790.
- [16] V. Dragović, M. Radnović, *Hyperelliptic Jacobians as billiard algebra of pencils of quadrics: Beyond Poncelet porisms*, Advances in Mathematics **219** (2008), no. 5, 1577–1607.
- [17] P. Griffiths, J. Harris, *A Poncelet theorem in space*, Comment. Math. Helvetici, **52** (1977), no. 2, 145–160.
- [18] P. Griffiths, J. Harris, *On Cayley's explicit solution to Poncelet's porism*, Enseign. Math. **24** (1978), no. 1–2, 31–40.
- [19] C. Jacobi, *Vorlesungen über Dynamic. Gesammelte Werke, Supplementband*, Berlin, 1884.

- [20] H. Knörrer, *Geodesics on the ellipsoid*, *Inventiones math.* **59** (1980), 119-143.
- [21] H. Knörrer, *Singular fibres of the momentum mapping for integrable Hamiltonian systems*, *J. Reine Angew. Math.* **355** (1985), 67-107.
- [22] V. V. Kozlov, D. V. Treshchëv, *Billiards*, Amer. Math. Soc., Providence RI, 1991.
- [23] H. Lebesgue, *Les coniques*, Gauthier-Villars, Paris, 1942.
- [24] J. Moser, *Geometry of quadrics and spectral theory*, The Chern Symposium, Springer, New York-Berlin, 1980, pp. 147-188.
- [25] J. Moser, A. P. Veselov *Discrete versions of some classical integrable systems and factorization of matrix polynomials*, *Comm. Math. Phys.* **139** (1991), no. 2, 217-243.
- [26] J. V. Poncelet, *Traité des propriétés projectives des figures*, Mett-Paris, 1822.
- [27] E. Previato, *Some integrable billiards*, in *SPT2002: Symmetry and Perturbation Theory*, S. Abenda, G. Gaeta and S. Walcher eds., World Scientific, Singapore, 2002, 181-195.
- [28] M. Radnović, V. Rom-Kedar, *Foliations of isonergy surfaces and singularities of curves*, *Regular and Chaotic Dynamics* **13** (2008), no. 6, 645-668.
- [29] E. Shlizerman, V. Rom-Kedar, *Hierarchy of bifurcations in the truncated and forced nonlinear Schrödinger model*, *Chaos* **15** (2005), no. 1.
- [30] H. Waalkens, H. R. Dullin, *Quantum Monodromy in Prolate Ellipsoidal Billiards*, *Annals of Physics* **295** (2002), no. 1, 81-112.

MATHEMATICAL INSTITUTE SANU, KNEZA MIHAILA 36, BELGRADE, SERBIA
MATHEMATICAL PHYSICS GROUP, UNIVERSITY OF LISBON, PORTUGAL
E-mail address: vladad@mi.sanu.ac.rs

MATHEMATICAL INSTITUTE SANU, KNEZA MIHAILA 36, BELGRADE, SERBIA
E-mail address: milena@mi.sanu.ac.rs